Pergamon

Geochimica et Cosmochimica Acta, Vol. 67, No. 19, pp. 3537–3546, 2003

0016-7037/03 $30.00 + .00

doi:10.1016/S0016-7037(00)00166-2

Measurement and interpretation of molecular-level forces of interaction between the siderophore azotobactin and mineral surfaces

TREAVOR A. KENDALL* and MICHAEL F. HOCHELLA, JR.

NanoGeoscience and Technology Laboratory, Department of Geological Sciences, Virginia Tech, Blacksburg, VA 24061, USA

(*Received August* 13, 2002; *accepted in revised form December* 31, 2002)

Abstract—The forces of interaction were measured between the siderophore azotobactin and the minerals goethite (α-FeOOH) and diaspore (α-AlOOH) in aqueous solution using force microscopy. Azotobactin, a pyoverdin-type siderophore, was covalently linked to a hydrazide terminated atomic force microscope tip using a standard active ester protein coupling technique. Upon contact with each mineral surface, the adhesion force between azotobactin and goethite was two to three times the value observed for the isostructural Al-equivalent diaspore. The affinity for the solid iron oxide surface reflected in the force measurements correlates with the specificity of azotobactin for aqueous ferric iron. Further, the adhesion force between azotobactin and goethite significantly decreases (4 nN to 2 nN) when small amounts of soluble iron (0.1 μM $FeCl_3 \cdot 6H_2O$) are added to the system at pH 3.5 suggesting a significant specific interaction between the chelating reactive center of azotobactin and the mineral surface. Changes in the force signature with pH and ionic strength were fairly predictable when considering mineral solubility, the charge character of the mineral surfaces, the molecular structure of azotobactin, and the intervening solution. For example, azotobactin–goethite adhesion values were consistently smaller at pH 3.5 relative to the forces at pH 7. At the lower pH, the large number of protons and the increase in the mineral solubility provides additional electron acceptors (e.g., H^+ and Fe^{3+}(aq)) that are free to compete for the basic oxygen chelating sites in the azotobactin structure. It is believed that this competition disrupts siderophore affinity for the surface resulting in decreased adhesion values.

1. INTRODUCTION

Siderophores are being recognized for their potential to influence geochemical processes in near surface systems. Given a widespread distribution, and the small, but relatively significant siderophore concentration in soils (Bossier et al., 1988; Hersman, 2000), the implications of siderophore–mineral interactions are far reaching. The influence of these interactions on mineral weathering and nutrient cycling, and the release of toxic constituents from mineral surfaces must be considered.

Siderophores are soluble, organic ligands released by microorganisms to chelate iron. The exceptional affinity ($K_f = 10^{20}$–10^{50}) siderophores exhibit for aqueous ferric iron allows many organisms to assimilate this essential nutrient in spite of the extremely low solubility of the solid iron forms that are dominant in oxidizing environments. Indeed, Page and Huyer (1984) document siderophore-producing bacteria successfully extracting ferric iron from minerals for growth and many studies have demonstrated dissolution of common iron oxides and silicates in the presence of siderophores (Seaman et al., 1992; Watteau and Berthelin, 1994; Hersman et al., 1995a,b; Holmen and Casey, 1996; Liermann et al., 2000; Maurice et al., 2000). Recent studies emphasize the role siderophores may have in contaminant fate and transport by providing quantitative evidence of their ability to affect the sorption of toxic metals and radionuclides on soil minerals (Kraemer et al., 1999, 2002; Neubauer et al., 2000).

Key to siderophore-influenced mineral dissolution and sorption/desorption reactions are the forces that bring the ligand into and out of contact with the mineral surface. It is well known that ligand-mineral interaction consists of a complex interplay between electrostatic, van der Waals, hydrophobic and steric forces that are dependent on the charge character and structure of the ligand and mineral surface, as well as the chemistry of the interstitial solution (Dzombak and Morel, 1990; Israelachvili, 1992; Stumm, 1992). Our objective is to extend the investigation of siderophore–mineral interaction to an extremely small dimensional scale by quantifying electrostatic and bonding forces. We utilize a novel force measuring technique called chemical force microscopy (CFM) (Noy et al., 1997). For the first time, we have directly measured the forces of interaction between a siderophore ligand and a mineral, in solution at the nano- to piconewton force sensitivity level. This information is used to determine if a siderophore can "differentiate" between a ferric iron-containing mineral and the aluminum-bearing isostructural equivalent; detect, quantify and characterize specific and nonspecific siderophore–mineral interactions under various solution conditions; predict surface association geometries based on the magnitude and pattern of the force data; and evaluate the possibility and nature of a siderophore-surface complex. In doing so, we hope to further define the role siderophores play in mineral dissolution and iron acquisition while opening up a new area of research that explores the forces of interaction between metal-specific ligands/biomolecules, and inorganic/mineral surfaces.

The siderophore azotobactin was selected as the model ligand to be attached to an atomic force microscope (AFM) tip in these force measurement experiments. Azotobactin is a relatively large (1.3 kDa), pyoverdin-type siderophore (Fig. 1) produced under iron limiting conditions by the nitrogen-fixing bacteria *Azotobacter vinelandii.* Other *A. vinelandii* sid-

* Author to whom correspondence should be addressed (tkendall@vt.edu).

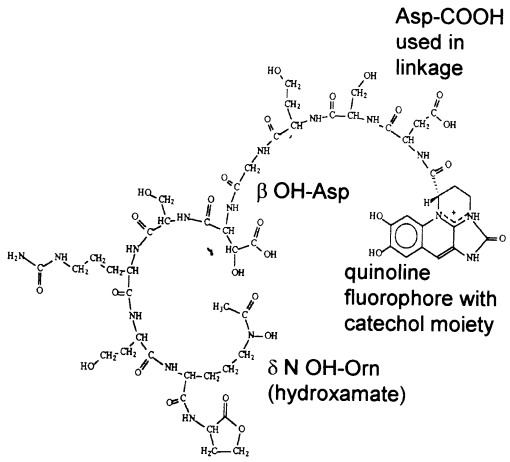

Fig. 1. Annotated azotobactin δ structure (adapted from Palanche et al., 1999).

erophores include the catecholates aminochelin, azotochelin and protochelin; however, all exhibit an affinity for ferric iron that is below azotobactin (Cornish and Page, 1998; Palanche et al., 1999). Azotobactin was targeted for these experiments because it is a natural product from an environmentally relevant bacterium; its structure and size facilitated covalent linkage to an AFM tip; the fluorescent quinoline chromophore at the base of its polypeptide backbone allows small concentrations of the molecule to easily be detected and quantified; and several studies on the coordination chemistry and kinetics of iron complexation exist (Hider, 1984; Demange et al., 1988; Winkelmann, 1991; Albrecht-Gary et al., 1995; Schaffner et al., 1996; Albrecht-Gary and Crumbliss, 1998). Finally, we were able to obtain an *A. vinelandii* mutant (F196; courtesy Dr. William Page, University of Alberta) that produces/hyper-produces azotobactin as its sole known siderophore, facilitating production and isolation (Sevinc and Page, 1992).

Goethite was selected for these experiments because it is the most abundant soil ferric iron oxide and is estimated to represent up to 70% of the total surface area available in a soil (Rakovan et al., 1999). Diaspore is a less common soil mineral, but was chosen because it is the isostructural Al-equivalent to goethite. Additionally, both mineral species were ideal for force measurements because single crystals with recognizable crystallographic faces presenting an optically flat surface could be obtained.

2. EXPERIMENTAL

2.1. Azotobactin Production and Isolation

Azotobactin was isolated from relatively large volumes of *A. vinelandii* F196 supernatant using a reverse phase chromatography procedure adapted from Demange et al. (1988). Briefly, multiple batches of 100 mL Fe-limited Burk media, pH 7.1, were inoculated with *A. vinelandii* F196 and incubated at 25°C with shaking at 200 rpm for 3–6 d. All glassware used during F196 growth and siderophore isolation was soaked overnight in 4 N HCl, then 50 mM EDTA and rinsed with Millipore water to minimize Fe contamination (Page, 1993). F196 cultures were removed from incubation when azotobactin concentrations reached ~150 mg/L (ε = 23500 mol/L^{-1} cm^{-1}) as determined with A380 measurements (pH 1.8) on a Beckman-Coulter DU 640 UV-Vis spectrophotometer. Two and a half (2.5) liters total culture were pooled and centrifuged at 36,400 *g* for 15 min. In 0.5 L batches, the supernatant containing the soluble azotobactin fraction was filtered (0.1 μm), adjusted to pH 4 using HCl and loaded on to a 19 cm × 2 cm reverse phase octadecyl silane (RP-18) preparative chromatography column using 0.05 M pyridine-acetic acid buffer, pH 5.0 (Demange et al., 1988). The column was flushed with 200 mL of 0.05 M buffer and azotobactin was then eluted with acetonitrile and buffer (1:1) at an average flow rate of 1 mL/min. The various fractions were scanned at A380 and those containing >15 mg/L azotobactin were pooled and loaded onto a 24 cm × 3.5 cm diethylaminoethyl (DEAE) cellulose column with 0.05 M pyridine-acetic acid buffer. The column was flushed with 200–250 mL of 0.05 M buffer and the azotobactin eluted with a linear gradient of 0.05 M–1 M pyridine–acetic acid buffer. Fractions containing >20 mg/L azotobactin were pooled, dried under N_2, resuspended in doubly deionized Millipore water (18 MΩ cm^{-1} Millipore water A10 system; Millipore Corp.), lyophilized and stored at −20°C. The purity of each separation fraction was monitored with reverse phase high performance liquid chromatography (HPLC) and UV-Vis spectrophotometry. In contrast to the filtered supernatant and RP-18 fractions, the HPLC spectra (380 nm) of the final azotobactin fraction consisted of a single, narrow peak with no shoulders at ~1.7 min (data not shown). Chrome Azurol-S (CAS) assays (Schwyn and Neilands, 1987), indicated consistent, robust siderophore activity in all fractions.

2.2. Tip Activation

Azotobactin molecules were linked to the AFM tip using an active ester cross-linking technique commonly used to couple two proteins (Staros et al., 1986; Grabarek and Gergely, 1990; Lahiri et al., 1999). In our scheme the azotobactin Asp carboxyl (see Fig. 1) was targeted for linkage with the amino group associated with a hydrazide terminated (-NH-NH$_2$) AFM tip (BioForce Labs). One (1) mg of lyophilized azotobactin was dissolved in 1 mL activation buffer (0.1 M MES; 0.5 M NaCl; pH 5). Taking advantage of the fact that pyoverdin siderophores complex Al^{3+} in the same octahedral coordination as it does with Fe^{3+}, but with a much lower affinity for Al (Hider, 1984; Mertz et al., 1991), azotobactin's oxygen ligands thought to participate in chelation (specifically those associated with the β-OH Asp) were protected before the linkage reaction by adding 110 μL of 1 M $AlCl_3$ (1:100 Azb:Al) to the solution and reacting for 20 min. Ten (10) μL each of 280 mM 1-Ethyl-3-(3-Dimethylaminopropyl) carbodiimide (EDC; Pierce) and 560 mM *N*-hydroyxsuccinimide (NHS; Pierce) was added and reacted for an additional 15 min. Exposure of the azotobactin's targeted carboxyl group to EDC in combination with NHS results in a stable, hydrolysis resistant, active succinimidyl ester that readily forms a peptide bond in the presence of an amino group. Here the amino group is supplied by the hydrazide terminated AFM tip which was submerged and mixed with the EDC-NHS solution. After 2 h at room temperature the tip was then removed and sequentially rinsed with 0.04 M EDTA (to remove the Al and regenerate the reactive groups), 10 mM NH_2OH, and Millipore water. The tip was allowed to incubate in each rinse solution for a minimum of 20 min. When not in use, activated tips were stored at 4°C in MES activation buffer at pH 5. Each activated tip was used within 24 h of preparation. Fluorescent images used to confirm the presence of azotobactin to the tip were collected on a Zeiss 510 Confocal Scanning Laser Microscope (CSLM) before and after the CFM experiments (Fig. 2).

2.3. Solution Conditions and Mineral Specimens

Force measurements were made in a Digital Instrument fluid cell filled with Millipore water adjusted to various pHs using HCl and NaOH, and ionic strengths using NaCl. The effect of soluble iron on the forces of interaction was also assessed. Baseline adhesion values between azotobactin and goethite were first collected with no iron added to the system. Successively increasing concentrations (0.001, 0.01, 0.1 μM) of $FeCl_3 \cdot 6H_2O$ were then introduced while monitoring the change in the force signatures. A final measurement was collected after an attempt to remove the added Fe^{3+}(aq) from the azotobactin chelating groups with a high concentration of a competing ligand (1 mM EDTA). Available data on the iron exchange kinetics between EDTA and azotobactin (Albrecht-Gary et al., 1995) were considered when

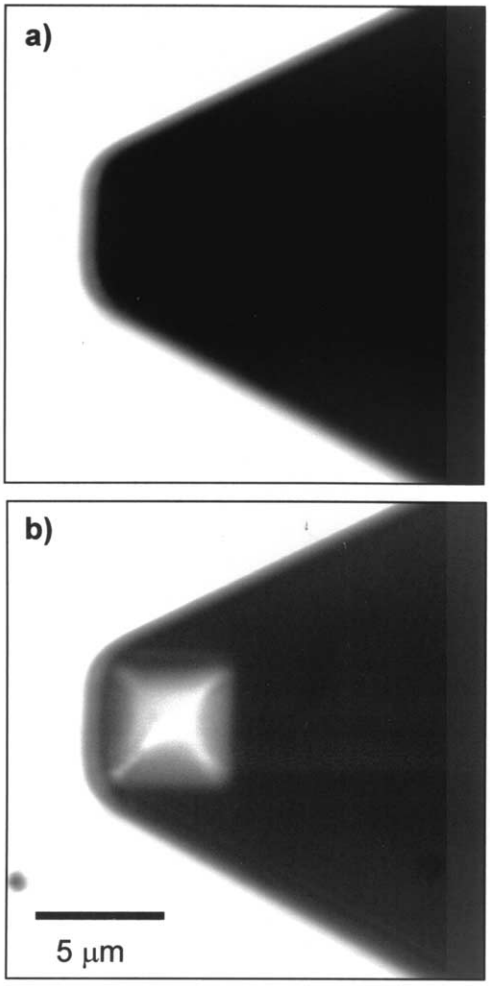

Fig. 2. Confocal Scanning Laser Image of an (a) unactivated AFM tip with no fluorescent signal evident, and (b) a tip activated with the inherently fluorescent azotobactin molecule. Images are a composite of two channels (Ch 1, 2) collected under a C-Apochromat 40×/1.2 water immersion objective. Ch 1 consists of transmitted light which provides a dark silhouette of the cantilever; Ch 2 uses a 505 nm long pass filter to collect fluorescence generated when the cantilever and tip are exposed to a UV laser (364 nm).

selecting the competing ligand concentration and tip immersion time. Specifically, the following equation was used to calculate a pseudo–first order rate constant (k_{obs}) at pH 3.5:

$$k_{obs} = \frac{K_1 K_2 k_3 [H^+]_0 [EDTA]_0}{1 + K_1[H^+]_0 + K_1 K_2 [H^+]_0 [EDTA]_0}$$

This relationship is derived from experimental data collected at pH 3.6–5.2 and EDTA concentrations ranging from 0.42–45 mM and assumes a three step ligand exchange mechanism where K_1 (1080 mol^{-1} L)and K_2 (0.008 mol^{-1} L) are equilibrium constants corresponding to the first two reactions: 1) protonation of the iron-azotobactin complex, and 2) the formation of an azotobactin-iron-EDTA complex. k_3 (500 s^{-1})is the first order rate constant of the final, rate limiting iron exchange reaction between azotobactin and EDTA. At pH 3.5, and an initial EDTA concentration of 1 mM ($k_{obs} = 1.0\times10^{-3}$ s^{-1}), the half-life of the pseudo–first order exchange reaction equals 11.5 min. Based on this we selected a minimum immersion period of 15 min to minimize the EDTA concentration in the system and to insure an effect could be observed within a reasonable time.

All solutions were exchanged after flushing the cell with 5–10 cell volumes of the new solution and the system was allowed to thermally stabilize (as monitored by drift in the photodiode signal) for a minimum of 15 min. The pH of the solutions was measured after the force measurements to monitor any changes in solution conditions during the experiments. Small (600–800 μm) single crystals of goethite (α-FeOOH) and diaspore (α-AlOOH) containing recognizable (010) faces with optically flat step terraces were carefully selected and cleaned using a series of acetone, methanol and Millipore water rinses immediately before force measurements (Stipp and Hochella, 1991).

2.4. AFM Operation and Data Processing

Force data were collected at room temperature on a NanoScope IIIa MutliMode SPM (Digital Instrument) at a cycle rate of 2 Hz over a 300 nm ramp with translation rates not exceeding 3 μm s^{-1}. Diode voltages were converted into cantilever deflection (nm) using the slope of the constant compliance region of the force curve. Cantilevers used in the experiments were triangular, 200 μm long, narrow legged and fixed with a pyramid shaped tip. Spring constants were determined by measuring the change in resonant frequency with added masses as described by (Cleveland et al., 1993). Deflection values were then converted into force using Hooke's Law. Force plots were generated by plotting force versus relative piezo movement or force versus tip-sample separation. A comprehensive description and discussion of AFM force plots is provided by (Cappella and Dietler, 1999).

A single force plot at a particular sample location does not always fully describe the force regime of a given interaction. As a result, force landscapes are often summarized by averaging single-point parameters identified in both the approach and retraction curve in a force plot. For example, once the tip and sample are in contact, the level of affinity that the molecules on the end of the AFM tip show for the surface is characterized by an average rupture or adhesion force, defined as a change in slope and/or minimum in the retraction force data. Likewise, a lack of affinity can be described by repulsion force values, often defined as local maxima in the approach data. Force curve processing and automated determination of these parameters, plus statistical calculations, whole force curve averaging, energy calculations and histogram generation was completed using a customized routine written by T. Kendall and H. Skulason for Igor Pro 4.04 (WaveMetrics, Inc.). The parameter extraction module quickly selects the values based on a set of given criteria such as maxima thresholds in the differentiated force data and tolerance limits for specific changes in slope.

A large number of force curves can be processed rapidly with the customized Igor routine, and, as a result, 120–150 curves were commonly collected at a single sample location. After examining histograms of the main parameters of interest (e.g., adhesion force, jump to contact distance), we found the data to be gaussian with a relatively low standard error. Experience showed that in most cases, a sample size of 60–70 force curves adequately described parameter distributions and means for our system. Most of the data collected were included in the averages and statistical analysis herein, with less than 3% of the curves from each sample location being excluded. Most of the eliminated curves contained a significant slope or periodic oscillation present in the region of no contact. This was believed to reflect a drift in the sample position due to a relaxation or shift of the fluid cell gasket and optical interference from stray laser light reflecting off of the mineral surface, respectively.

3. RESULTS AND DISCUSSION

3.1. Forces of Siderophore Interaction with an Iron Versus Aluminum Oxide

Significant differences exist in the forces of interaction between azotobactin and goethite, and azotobactin and diaspore. Most notable is the disparity in the attractive force associated with the approach; and the considerable difference in the force of adhesion upon retraction (Fig. 3a). The force associated with the jump to contact, an indicator of tip affinity for the surface, is on average 0.7 nN higher for goethite versus diaspore. Also

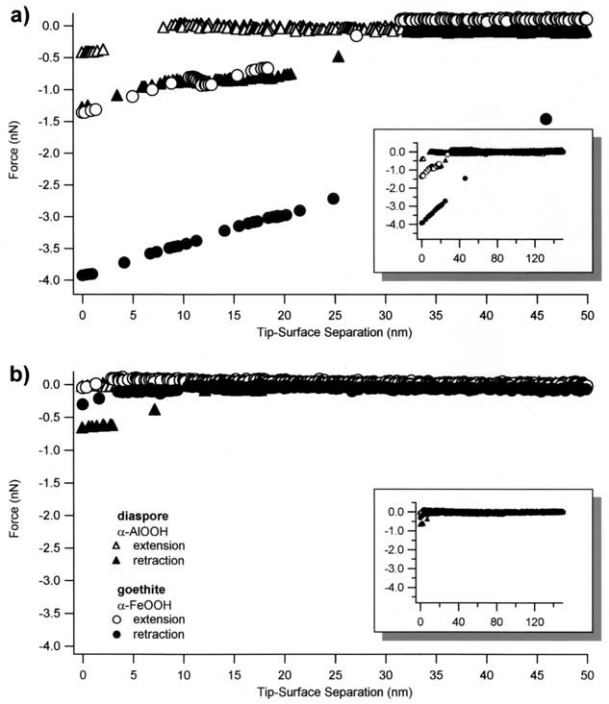

Fig. 3. Representative force–distance plots showing the interaction between the CFM tip and two minerals, diaspore (empty and filled triangles) and goethite (empty and filled circles). (a) Data collected using an azotobactin-activated tip. (b) Data collected with a control hydrazide terminated tip. Both force signatures were collected at pH 7; I = 10–1 M. Insets represent the same force plot, but with the x-axis range increased to show the region of no contact.

during approach the jump to contact distance at which the tip began to "feel" the surface is larger for goethite (~13 nm) than for diaspore (~6 nm). Upon retraction the average maximum force of adhesion between azotobactin and the iron oxide surface was consistently 2–3 times the value associated with the diaspore surface (Table 1). In contrast, control experiments with a hydrazide terminated tip lacking the azotobactin molecule produced similar force signatures for each mineral (Fig. 3b), indicating the large distinction between the diaspore and goethite forces are due to the presence of azotobactin and interference from the linker molecule is minimal.

Disparate populations in adhesion force values corresponding to different locations on a single mineral were observed. Figure 4 shows histograms of adhesion forces collected with the same tip at different sample locations on a goethite and diaspore surface. Changes in force with sample location reflect, in part, the influence of mineral microtopography on the force

Table 1. Comparison of average force parameters collected while probing azotobactin on diaspore and goethite

I = 10^{-1}M; pH 7	Diaspore	Goethite
F_{adh} (nN)	1.70 ± 0.21	3.58 ± 0.20
Retraction Energy (aJ)[a]	17.2 ± 3.6	69.9 ± 6.8
Jump to contact force (nN)	0.14 ± 0.06	0.81 ± 0.10

[a] aJ = 10^{-18} J.

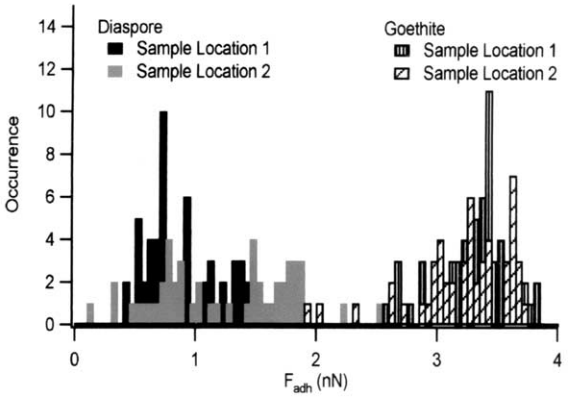

Fig. 4. Histogram showing variability in adhesion forces (Fadh) with mineral sample location. Sample locations were randomly selected.

measurements. Single (010) growth faces were probed, but it is likely that force measurements reflect to some degree the interaction between the azotobactin and surface features such as step edges and defects. Given the pN to nN sensitivity of this method it may be possible to capture the variation in surface reactivity associated with these features in the force signatures; however, definitive confirmation will require better constraint of the topography at each sample location. The observed variations due to microtopography, however, did not affect the overall force trends observed between goethite and diaspore.

3.2. Effect of Added Soluble Iron on Forces between Azotobactin and Goethite

The large adhesion force associated with goethite significantly decreased upon the successive addition of small concentrations of soluble iron ($FeCl_3 \cdot 6H_2O$) (Fig. 5). The lowered adhesion values then partially rebounded after the tip was immersed in 1 mM EDTA.

Albeit a qualitative observation, it should be noted that the 0.001 μM Fe(III) concentration detected in these force measurements is an order of magnitude below the detection limit

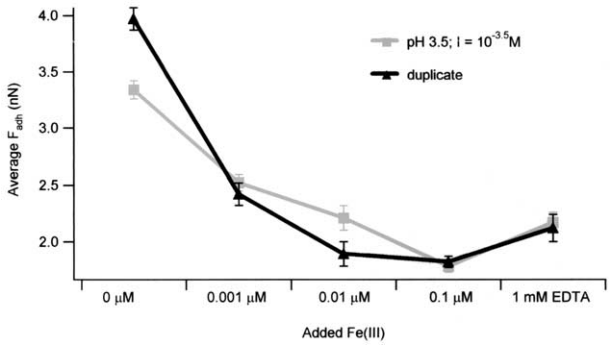

Fig. 5. Average adhesion force (Fadh) between azotobactin and goethite versus added ferric iron (as $FeCl3 \cdot 6H_2O$). The tip was immersed in each Fe concentration for a minimum 15 min and then rinsed thoroughly with Millipore water before collecting force measurements. Note the small rebound in adhesion values upon the addition of a small amount of EDTA. Fe(III) solids precipitation is not predicted at the selected pH (3.5) and maximum Fe concentrations (0.1 mM).

Table 2. Comparison of Fe(III) and A1(III) overall (1:1) formation constants (K_f) for selected siderophores and their component/analog ligands

Ligand	log K_f Fe(III)	log K_f AI(III)	pK_{a1}	pK_{a2}
Azotobactin[a]	28	NA	4–5	NA
Deferriferrioxamine B[b]	31	22	8.3	9.00
Catechol[c]	19	17	9.2	13
Hydroxycarboxylic acid[d]	3.6	0.85	5	>14
Acetohydroxamic acid[e]	11.5	8	8–10	—

Note: NA = not available.
[a] Palanche et al. (1999); Telford and Raymond (1996).
[b] pK_{a3} = 9.46, pK_{a4} = 10.84 (Crumbliss, 1991; Gaspar et al., (1999).
[c] Crumbliss (1991); Hider (1984).
[d] log K_f values are for lactic acid (Perrin, 1979; Telford and Raymond, 1996).
[e] Hider (1984); Nguyen-van-Duong et al. (2001).

reported when azotobactin is used as a spectrophotometric chemosensor for iron (Palanche et al., 1999). This speaks to the extreme sensitivity of this CFM technique, and further emphasizes the importance of minimizing iron contamination in the model system.

3.3. Assessment of the Azotobactin–Goethite/Diaspore Interaction

Collectively, the observations above suggest that the large adhesion values associated with the goethite surface reflect an affinity between the azotobactin on the tip and the iron associated with the goethite surface. The similarity in the point of zero charge for goethite (pzc = 7–9) (Cornell and Schwertmann, 1996; Kosmulski, 2001) and diaspore (pzc = 7–8) (Kosmulski, 2001) indicates the charge character of each surface on a large scale is comparable, with both being slightly positive to neutral at pH 7. A net negative charge is predicted on the azotobactin molecule (pK_a hydroxycarboxylate = 4–5; see Table 2), thus presenting a possible electrostatic or hydrogen bonding component to the interaction. It is possible our model systems deviate from pristine charge conditions causing a significant differential shift in the pzc values of the two minerals, such that the diaspore is negatively charged or neutral while goethite remains positively charged. This of course could result in a larger adhesion to the goethite surface. Three observations, however, indicate differences in surface charge alone do not satisfactorily explain the discrepancy in the goethite and diaspore force affinities. First, at pH 3.5, far from each mineral's pzc value, and where the azotobactin is predominantly fully protonated and neutral, we observe the same increase in adhesion for goethite over diaspore (see Section 3.5). Second, this relationship was also consistently observed when comparing data from several different locations on each mineral. This is in spite of changes in microtopography (discussed previously), or possible localized or anomalous charge distribution associated with each sample site. Finally, goethite force signatures collected at pH 7 often show a long range, electrostatic repulsion on approach that was equal to or significantly lower in the diaspore signatures collected under the same conditions and with the same tip (experiment 2; data not shown); yet, the goethite adhesion force averaged 3.81 nN compared to 1.38 nN for diaspore.

The observed force relationship likely reflects differences in the electronic character of each metal (e.g., Fe(III) versus Al(III)) contained in the mineral structure. The smaller ionic radius and electronegativity value of Al(III) predicts a lower affinity for the negative charges associated with the chelating oxygen groups. In contrast, the larger, more electronegative Fe(III) will behave as a harder acid with a higher affinity for the oxygens, presumably resulting in larger adhesion forces. A similar argument is used to explain the increased thermodynamic stability of the Fe(III)-siderophore complex (aq) compared to the Al(III)-complex (aq) (i.e., see DFAM Table 2) (Hider, 1984; Albrecht-Gary and Crumbliss, 1998). However, here the difference in formation constants between iron and aluminum is orders of magnitude (Table 2) which is in contrast to the 2-threefold change observed in the adhesion to each surface (Table 1). This discrepancy is difficult to explain, and one that can not be reconciled by the certain reduction in denticity associated with a siderophore-Fe(III) surface complex (Cocozza et al., 2002; Holmen and Casey, 1996) compared to the cognate hexadentate aqueous form. Assuming the adhesion force primarily reflects a monodentate interaction of the azotobactin hydroxamate group with each surface, there still exists a three order of magnitude increase in the stability of the acetohydroxamic acid(aH)-Fe(III) complex over the aH-Al(III) (Table 2). Schmitt et al. (2000), however, report a similar relationship between force measurements and thermodynamic constants. The average adhesion force associated with a nitriloacetic acid (NTA)-histidine (His) complex containing Cu^{2+} was 2.6 times the value associated with the NTA-His/Co^{2+} complex, yet the thermodynamic stability constant of the copper complex is over 3 orders of magnitude higher.

The addition of ferric chloride at pH 3.5 presents an available source of aqueous ferric iron primarily as Fe^{3+} and $Fe(OH)^{2+}$ ions that readily interact with the hydroxyl moieties believed to be involved in iron chelation (Fig. 1). With these reactive groups previously available for interaction with the surface now occupied by the iron, the force of attraction to the surface is decreased. This trend is reversed when EDTA is added, presumably removing the iron associated with the azotobactin. It is also possible that the rebound in adhesion values reflects the interaction between a ternary azotobactin-Fe(III)-EDTA complex with the surface. Albrecht-Gary et al. (1995) include the formation of a negatively charged ternary complex ($LH_3FeEDTA^-$) as an intermediate step in the exchange of iron from azotobactin to EDTA in solution which, if associated with the tip, could exhibit an attractive electrostatic force towards the positively charged goethite surface. The stability of this ternary complex, however, is relatively low. It is formed during an intermediate, fast (e.g., not rate limiting) reaction with an equilibrium constant (8.0×10^1 M) that is three orders of magnitude below the value of ferrioxamine B (2.4×10^4 M). The instability of the azotobactin-Fe-EDTA ternary complex is cited as one reason for azotobactin's fast exchange kinetics.

The effect of added soluble iron on adhesion values further demonstrates that an interaction between the azotobactin and the surface is being captured by this technique, but it also provides evidence that the siderophore is retaining a level of chelation activity when attached to the tip. The residual adhe-

sion that exists once the iron is added, however, raises interesting questions. Assuming complete coverage and a 1:1 linkage ratio (e.g., one azotobactin molecule linked to a single hydrazide group), the number of azotobactin molecules on the substrate including the tip and cantilever is on the order of 2.5×10^{11}. With a fluid cell volume of ca. 150 μL, this gives a maximum effective azotobactin concentration of 3 nM. At the higher iron concentrations of 0.01 and 0.1 μM the azotobactin concentration is exceeded by several orders of magnitude, suggesting that there is enough iron available to fully satisfy all of the azotobactin molecules. The flow through nature of the fluid cell also makes it unlikely that transport to the molecules on the tip could be limiting. The residual adhesion, however, may reflect interaction with some of the azotobactin groups that remain uncomplexed due to kinetic limitations. Or, if initial chelation of the soluble iron by a single oxygen ligand pair does occur, steric hindrances and changes in molecule conformation imposed by the linkage may prevent complete, octahedral coordination leaving additional ligand pairs free to interact with the surface. A final component of the residual adhesion could be attributed to nonspecific interactions between the surface and amino acid side chains or functional groups not involved in chelation, or between the surface and the chelated metal (i.e., as a ternary complex).

3.4. Details of Force Curve Features

Typical force curves display a single, discrete rupture event (Fig. 3a), in the force regime of 3–5 nN at a loading rate of 120 nN s^{-1} upon retracting from the goethite surface (in the absence of added iron). This feature was consistently observed across disparate experiments using different tips indicating that a similar interaction was reproducibly captured. Using a tip surface interaction geometry described by Derjaguin, Muller and Topov (DMT) theory, which assumes no deformation and a zero contact area upon bond rupture, and a nominal tip curvature radius of 40 nm, the estimated contact area for these experiments is 0.003 μm^2 (Noy et al., 1997; Stout, 2001). Spacing between the individual self-assembled monolayer (SAM) groups that anchor each azotobactin molecule to the tip is estimated to be 5–10 angstroms (Lahiri et al., 1999; Kondoh et al., 2001). At a linkage reaction yield of 100% (Grabarek and Gergely, 1990), this puts the number of molecules in contact with the surface on the order of a few thousand. With no way of determining how many of these potential interactions contribute to the observed forces in a single force curve, it is difficult to comment on the type of interaction that is being disrupted upon retraction (i.e., covalent, ionic, noncovalent, etc.). Grandbois et al. (1999) report similar force values for the rupture of a covalent bond, however, their loading rate was an order of magnitude lower (10 nN s^{-1}) and, un-like this study, their experiment was specifically designed to capture single molecule interactions.

Hundreds of force curves were collected at a single sample location over sampling periods ranging from 10 to 50 min. During this time adhesion force values for both diaspore and goethite fluctuated in a random fashion about the mean (2σ = 10%) with no discernible time dependence. The consistency of the values suggests that the interacting groups associated with the molecule and the surface remained relatively unchanged after each measurement, and that the bonds that were being disrupted during retraction did not systematically affect subsequent measurements. In contrast to disrupting preexisting structural bonds associated with the siderophore molecule or mineral surface, the data suggest that each rupture event recorded in sequence represents the breakage of bonds/interactions that were formed and broken during a single approach and retraction cycle.

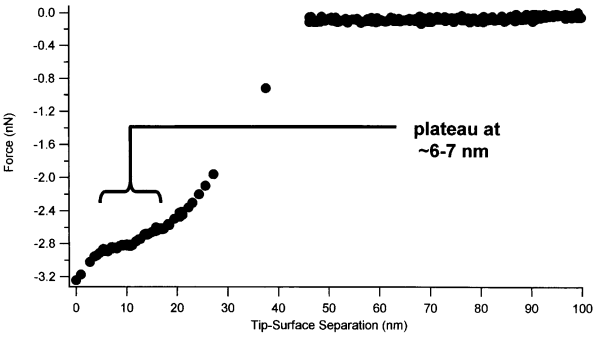

Fig. 6. Retraction curve showing plateau that is commonly observed in force signatures collected with azotobactin activated tips. It is suggested that this feature may represent the extension of the azotobactin and linker molecule during separation from the mineral surface.

A clue as to which siderophore functional group is interacting with the surface can be found in a distinctive plateau that is present in many of the retraction curves near the jump from contact. Here, the force slope remains constant over the initial 6–7 nm of retraction (Figs. 6 and 7) and then plateaus as energy is being absorbed. This is interpreted as the extension of the siderophore and linker molecules attached to the mineral surface in parallel. Given the linkage geometry shown in Figure 7, the dimensions of the plateau require that the azotobactin molecule be associated with the surface via groups at the C-terminus of the molecule, specifically the homoserine lactone or the hydroxamate group associated with the δ OH-ornithine residue. This is based on calculations that assume an extended length of 0.38 nm for each amino acid (Garrett and Grisham, 1999) and an additional 3 nm added for the 11 carbon hydrazide terminated linker molecule. Reports that the azotobactin hydroxamate group initiates chelation in aqueous systems (Telford and Raymond, 1996; Albrecht-Gary and Crumbliss, 1998) coupled with its terminal position on the molecule, further strengthens the idea that this group is a dominant component during surface interaction.

3.5. Ionic Strength and pH Effects on the Forces of Interaction

Observed force relationships, specifically the enhanced rupture forces between azotobactin and goethite, were reproducible in both duplicate experiments, and under various solution conditions (Fig. 8; Table 3). However, a closer examination of changes in the forces with pH and ionic strength provides additional information on the nature of the siderophore–mineral interaction and its dependence on electrostatics, mineral surface charge and solubility, and proton equilibria.

First, general trends with pH and ionic strength are identified

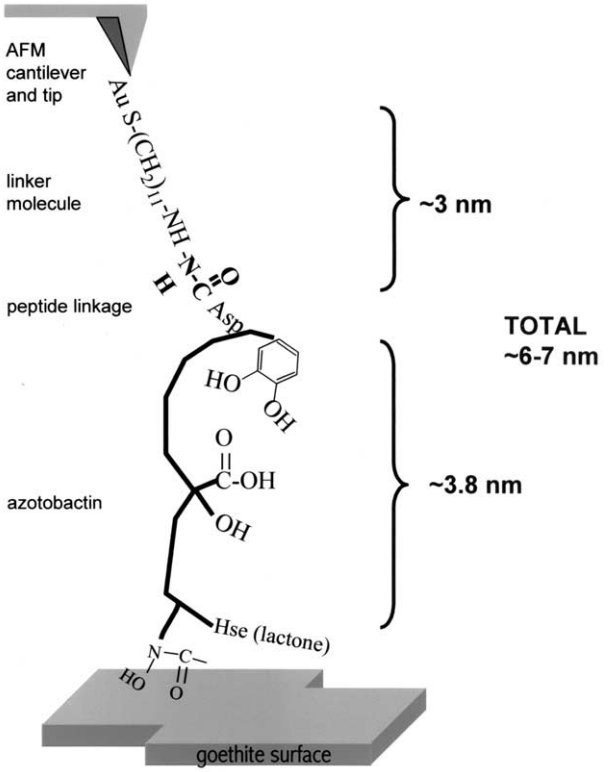

Fig. 7. Schematic showing extension of the azotobactin molecule during retraction from the mineral surface. Note the geometry and nature of the peptide linkage that joins the molecule to the AFM tip. Not to scale.

by comparing results from all data sets independently generated during this study. A more controlled experiment where a single activated tip was probed on goethite while multiple solutions were exchanged from the fluid cell then allowed us to study, in detail, the dependence of these forces on the charge character of the biomolecule mineral interface.

In the separate experiments run up to several months apart, the adhesion force ratio between goethite and diaspore ranged from 2.1 to 3.6 under various pH and ionic strengths (Table 3). A notable increase in the goethite/diaspore adhesion ratio is

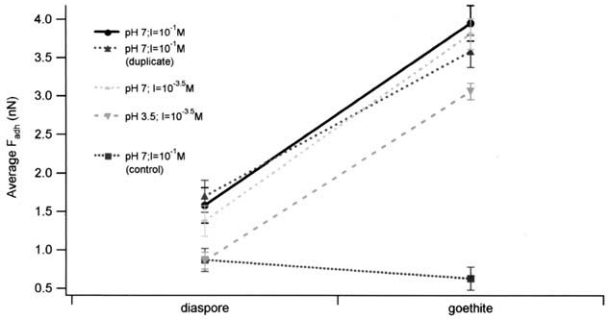

Fig. 8. Average adhesion forces (Fadh) for goethite and diaspore collected with azotobactin-activated tip under various solution conditions. Control values collected with only a hydrazide terminated tip are added for reference.

Table 3. Ratios of average adhesion force for goethite and diaspore (F_{adh} goethite/F_{adh} diaspore) under various solution conditions

Experiment	Ionic strength (M)	pH	$F_{adh\ goethite}$/ $F_{adh\ diaspore}$
1	10^{-1}	7	3.95/1.58 = 2.5
1 (duplicate)	10^{-1}	7	3.58/1.70 = 2.1
2	$10^{-3.5}$	7	3.81/1.38 = 2.7
3	$10^{-3.5}$	3.5	3.06/0.86 = 3.6
4 control (no azotobactin)	10^{-1}	7	0.63/0.87 = 0.7

evident with decreasing pH and appears to be driven by a larger drop in the diaspore adhesion values. Going from pH 7 to 3.5 diaspore values decrease on average by 43% compared to 20% for goethite. A disparity also exists when comparing the solubilities of each mineral with pH (3–7) where the change in diaspore solubility is ~3 orders of magnitude higher than the change in goethite solubility. This dictates that as the pH is lowered, more Al(aq) relative to Fe(aq) will become available to satisfy azotobactin's reactive groups and thereby disproportionately disrupt its affinity for the diaspore surface. Similar to the results when soluble iron was added, this technique again demonstrates its ability to capture subtle changes in solution composition at the biomolecule-mineral interface. However, caution must be taken when making absolute comparisons of data sets collected with different tips and mineral samples. Differences in force magnitudes can be produced by relative disorder of the SAM associated with each tip (Ito et al., 1999). And, although many steps were taken to minimize iron contamination, clearly with the extreme selectivity and sensitivity of azotobactin for Fe(III), even in minute concentrations (this study; Palanche et al., 1999), unforeseen, minimal amounts of iron could alter force values and must be considered.

To further comment on the effect of pH and ionic strength while minimizing the variability associated with data from different tips, an experiment with a single activated tip probed on goethite under various solution conditions was conducted. Representative force curves collected under four different solution conditions (Fig. 9) show subtle but important effects on the forces of interaction. An increase in ionic strength at constant pH (compare Figs. 9a and 9b) results in a shortened jump

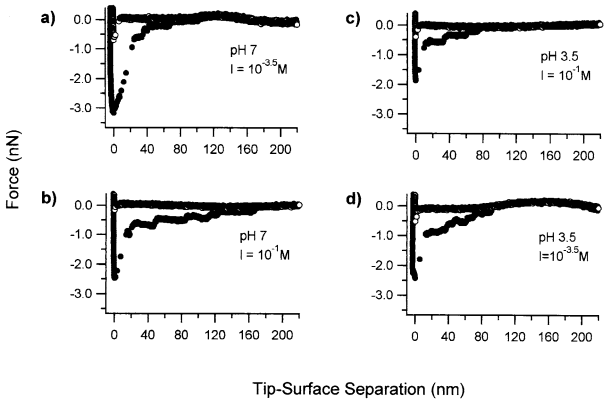

Fig. 9. Effect of pH and ionic strength on the azotobactin–goethite force signature. See text for details.

to contact distance during approach. A similar decrease in the range of interaction with decreased Debye length has been observed in other force measurements (Noy et al., 1997; Lower et al., 2000) and is attributed to the collapse of the electrical double layer associated with the surface (Israelachvili, 1992; Noy et al., 1997). The small decrease in adhesion shown in Figure 9b could reflect the small increase in goethite solubility at higher ionic strengths (Hsu and Marion, 1985; Cornell and Schwertmann, 1996), but is more likely connected with changes in the electrostatic component of the interaction. A decrease in the long-range attractive force on approach (jump to contact; compare Figs. 9a and 9b) with increasing ionic strength confirms the interaction's susceptibility to changes in the ionic character of the intervening solution. Specifically, the forces drop because the decreased positive surface potential of the goethite at the higher ionic strength (0.1 M) (Stumm, 1992) reduces the relative affinity of the negatively charged azotobactin for the surface. Yao and Yeh (1996) invoke a similar argument to explain a drop in the adsorption of smaller ionizable organic ligands (e.g., fumarate and malate) onto δ-Al_2O_3 with higher ionic strengths.

Lower adhesion values were recorded at pH 3.5 (Fig. 9c) relative to pH 7; an observation that was consistently made throughout this study (e.g., see Fig. 8, Table 3). The additional soluble iron resulting from the 4–5 orders of magnitude increase in goethite solubility at pH 3.5 likely contributes to the decline in adhesion; however, additional lability may also result from proton competition. At lower pH more protons are available to compete with Fe(III) as a hard acid for the basic, oxygen ligands in the siderophore structure (Crumbliss, 1991). The result is a disruption of azotobactin's affinity for the surface and lowered adhesion values. A change in ionic strength from 0.1 M to $10^{-3.5}$ M at pH 3.5 shows a small rebound in adhesion values (Fig. 9d). As expected, the change in adhesion values with a change in ionic strength at pH 7 is not present at pH 3.5, where the molecule is predominantly neutral.

4. SUMMARY AND CONCLUSIONS

This study has demonstrated the ability of force microscopy to detect the interaction between siderophores and metals contained on mineral surfaces. Specifically, it is believed that the strong adhesion force between azotobactin and goethite is generated by an attraction, both specific and electrostatic (esp. at pH 7) in nature, between chelating groups of azotobactin and the iron contained on the surface of a mineral. This observation alone has implications on the role of azotobactin in mineral dissolution. Page and Huyer (1984) and Page and Grant (1988) have indicated azotobactin works in combination with the smaller ligand dihydroxybenzoic acid (DHBA) to acquire iron from a mineral source. The mechanism they propose begins with DHBA release of Fe^{3+}(s) from the mineral via reductive dissolution followed by a transfer of Fe^{3+}(aq) to the higher affinity ligand azotobactin and ultimately back to the cell. Studies with other siderophores provide evidence of a possible binary or ternary system for iron transfer from the mineral to the microorganism, including the recent observation of a positive, synergistic effect of desferrioxamine-B with oxalate on goethite dissolution rates (Cervini-Silva and Sposito, 2002). This scenario downplays the siderophore surface interaction of larger ligands, instead relegating the high molecular weight hexadentate chelators (e.g., azotobactin) to a shuttle in solution that uses its superior chelating ability to scavenge iron from bidentate ligands. While dissolution facilitated by this multiligand mechanism is feasible, the force evidence demonstrating azotobactin's strong surface affinity presents the distinct possibility of a relatively large siderophore entering into a complex with the mineral surface. Further, steric constraints imposed by ligand size, structure and conformation, together with the limited access to an iron atom contained on a mineral surface, would certainly preclude hexadentate coordination with the surface (Hersman, 2000). Instead, our force data suggest a coordination formed by oxygen pairs that terminate the azotobactin molecule as one possibility. This observation supports the notion that adsorption and surface complexes are less dependent on ligand structure than aqueous complex formation (Stone, 1997). Evidence of surface complexes involving other siderophores and ligands, albeit much smaller than azotobactin, has also been found with Fourier transform infrared (FT-IR) (Hansen et al., 1995; Holmen and Casey, 1996) and X-ray photoelectron (XPS) (Kalinowski et al., 2000) spectroscopy.

This CFM technique allows us to directly monitor ligand-surface interaction under environmentally relevant conditions with pico- to nanonewton force resolution and a spatial resolution of tens of nanometers down to potentially the atomic level. While investigating the effect of solution conditions on this interaction, it became apparent that the sensitivity of this technique also allows small changes in mineral solubility and associated metal concentrations, pH, and ionic strength to be detected, opening up the possibility of using this technique to detect localized solution micro- or even nanoenvironments associated with a surface.

Force maps that display the spatial distribution of lateral force values which correspond to different levels of tip-sample interaction are also possible with this technique (Noy et al., 1997). Here, a tip activated with a ligand specific for a particular metal (e.g., the siderophore and Fe(III) system) is rastered across a mineral surface. Large adhesion forces associated with areas on the mineral where the complementary metal is found in high concentration, as either a sorbed or structural species, would then provide the contrast necessary to image the metal's spatial distribution. Such images could be useful for identifying contaminant distribution on a surface or pinpointing impurity concentrations on a mineral growth face. Because a near continuum of force values is necessary to generate a complete force map, this technique requires the ligand to remain relatively unaltered upon interaction with the metal or the surface. This appears to be the case for azotobactin based on the lack of a discernible time dependence of the forces detected over hundreds of measurements.

Parallels may be drawn between predictable trends in forces measured between a ligand and a mineral with trends in ligand adsorption behavior. Briefly, adhesion values between a ligand-activated tip and a mineral could be collected over a given pH range. A plot of these values could then be compared with an adsorption edge for the same ligand over the same pH range in an effort to assess the level of correlation between force measurements and adsorption. For example, a rise in adsorption that is not explained by protonation or deprotonation of the

ligand or surface may be explained by a short-range specific interaction recorded as an increase in adhesion force.

The concentration of the siderophore or ligand attached to the tip dictates the number of groups interacting with the surface, and ultimately, the absolute force values of the interaction (Florin et al., 1994; Schmitt et al., 2000). To capture consistent force and energy values at the ligand-mineral interface that can be compared across model systems, the next challenge will be to work towards single molecule force measurements—a task that becomes increasingly difficult with decreasing molecular weight of the molecule of interest. Such measurements have the potential to add to the broad, load-dependent energy landscape (Merkel et al., 1999) that is used to describe the nature of the bonds that are being ruptured upon retraction of the ligand from the mineral.

Acknowledgments—We thank S. Lower (U. of Maryland), L. Hersman (Los Alamos National Lab), C. Tadanier and the remainder of Virginia Tech mineral-microbe/NIRT group including M. Potts, A. Madden, T. Cail, S. E. O'Reilly, C. Airey, A. Doernte for lab assistance, useful discussions, and early reviews of this manuscript. J. Jerz and J. D. Rimstidt also contributed helpful comments and suggestions. F. Rabel and B. Lower provided assistance in modifying the chromatography method, F. Etzkorn and P. Deck assisted in developing the protein linkage scheme and K. DeCourcy provided CSLM support. The manuscript was improved with the comments of two anonymous reviewers. HPLC analysis was completed by E. Smiley (CEE, Virginia Tech). This research was funded by a GAAN Fellowship (U.S. Department of Education) awarded to T. Kendall, NSF's Nanoscale Science and Engineering (NSE) Program (EAR 01-03053), and the Department of Energy's OBES Geosciences Program (DE-FG02-99ER 15002).

Associate editor: G. Sposito

REFERENCES

Albrecht-Gary A.-M., Palanche-Passeron T., Rochel N., Hennard C., and Abdallah M. A. (1995) Bacterial siderophores: Iron exchange mechanism with ethylenediaminetetraacetic acid. *New J. Chem* **19,** 105–13.

Albrecht-Gary A. -M. and Crumbliss A. L. (1998) Coordination chemistry of siderophores: Thermodynamics and kinetics of iron chelation and release. In *Iron Transport and Storage in Microorganisms, Plants, and Animals*, Vol. 35 (eds. A. Sigel and H. Sigel), pp. 239–327. Marcel Dekker.

Bossier P., Hofte M., and VerstraeteW. (1988) Ecological significance of siderophores in soil. In *Advances in Microbial Ecology*, Vol. 10 (ed. K. C. Marshall), pp. 385–414. Plenum Press.

Cappella B. and Dietler G. (1999) Force–distance curves by atomic force microscopy. *Surf. Sci. Rep* **34,** 1–104.

Cervini-Silva J. and Sposito G. (2002) Steady-state dissolution kinetics of aluminum–goethite in the presence of desferrioxamine-B and oxalate ligands. *Environ. Sci. Technol* **36,** 337–342.

Cleveland J. P., Manne S., Bocek D., and Hansma P. K. (1993) A nondestructive method for determining the spring constant of cantilevers for scanning force microscopy. *Rev. Sci. Instruments* **64,** 403–405.

Cocozza C., Tsao C. C. G., Cheah S. F., Kraemer S. M., Raymond K. N., Miano T. M., and Sposito G. (2002) Temperature dependence of goethite dissolution promoted by trihydroxamate siderophores. **66**, 431–438.

Cornell R. M. and Schwertmann U. (1996) *The Iron Oxides: Structure, Properties, Reactions, Occurrence and Uses*. VCH.

Cornish A. S. and Page W. J. (1998) The catecholate siderophores of *Azotobacter vinelandii*: Their affinity for iron and role in oxygen stress management. *Microbiol. Uk* **144,** 1747–1754.

Crumbliss A. L. (1991) Aqueous solution equilibrium and kinetic studies of iron siderophore and model siderophore complexes. In *CRC Handbook of Microbial Iron Chelates* (ed. G. Winkelmann), pp. 177–235. CRC Press.

Demange P., Bateman A., Dell A., and Abdallah M. A. (1988) Structure of azotobactin d, a siderophore of *Azotobacter vinelandii* strain-D (Ccm-289). *Biochemistry* **27,** 2745–2752.

Dzombak D. A. and Morel F. M. M. (1990) *Surface Complexation Modeling: Hydrous Ferric Oxide*. Wiley-Interscience.

Florin E. L., Moy V. T., and Gaub H. E. (1994) Adhesion forces between individual ligand-receptor pairs. *Science* **264**(5157), 415–417.

Garrett R. H. and Grisham C. M. (1999) *Biochemistry*. Saunders College Publishing.

Gaspar M., Grazina R., Bodor A., Farkas E., and Santos M. A. (1999) Siderophore analogues: A new macrocyclic tetraamine tris(hydroxamate) ligand; synthesis and solution chemistry of the iron(III), aluminium(III) and copper(II) complexes. *J. Chem. Soc. Dalton Trans.* **5,** 799–806.

Grabarek Z. and Gergely J. (1990) Zero-length crosslinking procedure with the use of active esters. *Anal. Biochem* **185,** 131–5.

Grandbois M., Beyer M., Rief M., Clausen-Schaumann H., and Gaub H. E. (1999) How strong is a covalent bond? *Science* **283**(5408), 1727–1730.

Hansen D. C., McCafferty E., Lins C. W., and Fitzpatrick J. J. (1995) An FT-IR investigation of parabactin adsorbed onto aluminum. *Appl. Surf. Sci* **84,** 85–90.

Hersman L. E. (2000) The role of siderophores in iron oxide dissolution. In *Environmental Microbe–Metal Interactions* (ed. D. R. Lovley), pp. 395. ASM Press.

Hersman L., Lloyd T., and Sposito G. (1995a) Siderophore-promoted dissolution of hematite. *Geochim. Cosmochim. Acta* **59,** 3327–3330.

Hersman L., Maurice P., and Sposito G. (1995b) Iron acquisition from hematite by an aerobic *Pseudomonas* sp. *Abstr. Papers Am. Chem. Soc.* **209,** 94-GEOC.

Hider R. C. (1984) Siderophore mediated adsorption of iron. In *Structure and Bonding,*Vol. 58, *Siderophores from Microorganisms and Plants*, pp. 25–87.

Holmen B. A. and Casey W. H. (1996) Hydroxamate ligands, surface chemistry, and the mechanism of ligand-promoted dissolution of goethite [a-FeOOH(s)]. *Geochim. Cosmochim. Acta* **22,** 4403–4416.

Hsu P. H. and Marion G. (1985) The solubility product of goethite. *Soil Sci* **140,** 344–51.

Israelachvili J. N. (1992) *Intermolecular and Surface Forces*. Academic Press.

Ito T., Citterio D., Buehlmann P., and Umezawa Y. (1999) Observation of silver and hydrogen ion binding to self-assembled monolayers using chemically modified AFM tips. *Langmuir* **15,** 2788–2793.

Kalinowski B. E., Liermann L. J., Brantley S. L., Barnes A., and Pantano C. G. (2000) X-ray photoelectron evidence for bacteria-enhanced dissolution of hornblende. *Geochim. Cosmochim. Acta* **64,** 1331–1343.

Kondoh H., Saito N., Matsui F., Yokoyama T., Ohta T., and Kuroda H. (2001) Structure of alkanethiolate monolayers on Cu(100): Self-assembly on the four-fold-symmetry surface. *J. Phys. Chem. B* **105,** 12870–12878.

Kosmulski M. (2001) *Chemical Properties of Material Surfaces*. Marcel Dekker.

Kraemer S. M., Cheah S. F., Zapf R., Xu J. D., Raymond K. N., and Sposito G. (1999) Effect of hydroxamate siderophores on Fe release and Pb(II) adsorption by goethite. *Geochim. Cosmochim. Acta* **63,** 3003–3008.

Kraemer S. M., Xu J. D., Raymond K. N., and Sposito G. (2002) Adsorption of Pb(II) and Eu(III) by oxide minerals in the presence of natural and synthetic hydroxamate siderophores. *Environ. Sci. Technol.* **36,** 1287–1291.

Lahiri J., Isaacs L., Tien J., and Whitesides G. M. (1999) A strategy for the generation of surfaces presenting ligands for studies of binding based on an active ester as a common reactive intermediate: A surface plasmon resonance study. *Anal. Chem* **71,** 777–790.

Liermann L. J., Kalinowski B. E., Brantley S. L., and Ferry J. G. (2000) Role of bacterial siderophores in dissolution of hornblende. *Geochim. Cosmochim. Acta* **64,** 587–602.

Lower S. K., Tadanier C. J., and Hochella M. F. (2000) Measuring interfacial and adhesion forces between bacteria and mineral sur-

faces with biological force microscopy. *Geochim. Cosmochim. Acta* **64,** 3133–3139.

Maurice P. A., Lee Y. J., and Hersman L. E. (2000) Dissolution of Al-substituted goethites by an aerobic *Pseudomonas mendocina* varbacteria. *Geochim. Cosmochim. Acta* **64,** 1363–1374.

Merkel R., Nassoy P., Leung A., Ritchie K., and Evans E. (1999) Energy landscapes of receptor-ligand bonds explored with dynamic force spectroscopy. *Nature* **397,** 50–53.

Mertz C., Demange P., Marraud M., Dell A., Linget C., Abdallah M. A., and Chang M. T. (1991) Conformational study of the aluminum (III)-pyoverdin complex from Pseudomonas aeruginosa by proton 2D NMR techniques. Pept. 1990. Proc. Eur. Pept. Symp., 21st, 543–4.

Neubauer U., Nowack B., Furrer G., and Schulin R. (2000) Heavy metal sorption on clay minerals affected by the siderophore desferrioxamine B. *Environ. Sci. Technol.* **34,** 2749–2755.

Nguyen-van-Duong M. K., Guillot V., Nicolas L., Gaudemer A., Lowry L., Spasojevic I., and Crumbliss A. L. (2001) Synthesis, ligand pK(a), and Fe(III) complexation constants for a series of bipodal dihydroxamic acids. *Inorg. Chem.* **40,** 5948–5953.

Noy A., Vezenov D. V., and Lieber C. M. (1997) Chemical force microscopy. *Annu. Rev. Mater. Sci.* **27,** 381–421.

Page W. J. (1993) Growth conditions for the demonstration of siderophores and iron-repressible outer membrane proteins in soil bacteria, with an emphasis on free-living diazotrophs. In *Iron Chelation in Plants and Soil Microorganisms* (eds. L. L. Barton and B. C. Hemming), pp. 76–108. Academic Press.

Page W. J. and Huyer M. (1984) Derepression of the *Azotobacter vinelandii* siderophore system, using iron-containing minerals to limit iron repletion. *J. Bacteriol* **158,** 496–502.

Page W. J. and Grant G. A. (1988) Partial repression of siderophore-mediated iron transport in *Azotobacter vinelandii* grown with mineral iron. *Can. J. Microbiol* **34,** 675–9.

Palanche T., Marmolle F., Abdallah M. A., Shanzer A., and Albrecht-Gary A. M. (1999) Fluorescent siderophore-based chemosensors: Iron(III) quantitative determinations. *J. Biol. Inorg. Chem.* **4,** 188–198.

Perrin D. D. (1979) *Stability Constants of Metal–Ion Complexes, Part B: Organic Ligands.* Pergamon Press.

Rakovan J., Becker U., and Hochella M. F. Jr. (1999) Aspects of goethite surface microtopography, structure, chemistry, and reactivity. *Am. Mineral.* **84,** 884–894.

Schaffner E. M., Hartmann R., Taraz K., and Budzikiewicz H. (1996) Structure elucidation of Azotobactin 87, isolated from *Azotobacter vinelandii* ATCC 12837. *Z. Nat. C J. Biosci.* **51,** 139–150.

Schmitt L., Ludwig M., Gaub H. E., and Tampe R. (2000) A metal-chelating microscopy tip as a new toolbox for single-molecule experiments by atomic force microscopy. *Biophys. J.* **78,** 3275–3285.

Schwyn B. and Neilands J. B. (1987) Universal chemical assay for the detection and determination of siderophores. *Anal. Biochem* **160,** 47–56.

Seaman J. C., Alexander D. B., Loeppert R. H., and Zuberer D. A. (1992) The availability of iron from various solid-phase iron sources to a siderophore producing *Pseudomonas* strain. *J. Plant Nutr.* **15,** 2221–2233.

Sevinc M. S. and Page W. J. (1992) Generation of *Azotobacter vinelandii* strains defective in siderophore production and characterization of a strain unable to produce known siderophores. *J. Gen. Microbiol.* **138,** 587–596.

Staros J. V., Wright R. W., and Swingle D. M. (1986) Enhancement by *N*-hydroxysulfosuccinimide of water-soluble carbodiimide-mediated coupling reactions. *Anal. Biochem* **156,** 220–2.

Stipp S. L. and Hochella M. F. Jr. (1991) Structure and bonding environments at the calcite surface as observed with X-ray photoelectron spectroscopy (XPS) and low energy electron diffraction (LEED). *Geochim. Cosmochim. Acta* **55,** 1723–36.

Stone A. T. (1997) Reactions of extracellular organic ligands with dissolved metal ions and mineral surface. In *Geomicrobiology: Interactions between Microbes and Minerals.*, Vol. 35 (eds. J. F. Banfield and K. H. Nealson), pp. 309–341. Mineralogical Society of America.

Stout A. L. (2001) Detection and characterization of individual intermolecular bonds using optical tweezers. *Biophys. J.* **80,** 2976–2986.

Stumm W. (1992) *Chemistry of the Solid–Water Interface: Processes at the Mineral–Water and Particle–Water Interface in Natural Systems*. Wiley-Interscience.

Telford J. R. and Raymond K. N. (1996) Siderophores. *Comp. Supramol. Chem.* **1,** 245–266.

Watteau F. and Berthelin J. (1994) Microbial dissolution of iron and aluminum from soil minerals—Efficiency and specificity of hydroxamate siderophores compared to aliphatic-acids. *Eur. J. Soil Biol.* **30,** 1–9.

Winkelmann G. (1991) *CRC Handbook of Microbial Iron Chelates.* CRC Press.

Yao H.-L. and Yeh H.-H. (1996) Fumarate, maleate, and succinate adsorption on hydrous δ-Al_2O_3. 2. Electrophoresis observations and ionic-strength effects on adsorption. *Langmuir* **12,** 2989–2994.